Three Dimensional Surface Reconstruction using Scanning Electron Microscopy and the Design of a Nanostructured Electron Trap

Renke Scheuer[a], Eduard Reithmeier[a]

[a]Institute of Measurement and Automatic Control, Leibniz Universität Hannover

Nienburger Str. 17, 30167 Hannover, Germany, E-Mail: sekretariat@imr.uni-hannover.de

ABSTRACT

This paper gives an overview of the possible methods for a three-dimensional surface acquisition in the micrometer scale. It is pointed out that Scanning Electron Microscopy is a capable method for measurement tasks of this kind; therefore, it presents possible ways for implementing this technique in a three-dimensional surface reconstruction. The improved photometric method promises the best performance; its further implementation is developed and explained. Therefore, some modifications of the employed Scanning Electron Microscope (SEM) are described, for instance, the integration of two supplemental detectors, a modified collector grid and a gun shielding. All modifications were evaluated using FEM-Simulations before their implementation. A signal mixing is introduced in order to still be able to use the improved photometric method with four detectors in spite of the fact that it was designed for a two-detector system. For verification purposes, a sphere normal is measured by means of the modified system. It can be seen that the maximal detectable slope angle could be increased compared to the old photometric method. In addition, we introduce an electron trap consisting of nano structured titanium. The structure is tested regarding its ability to catch electrons of different energies and compared to non structured titanium. The trap can later be implemented on the bottom of the electron gun to catch unwanted backscattered electron (BSE) emission which could otherwise affect the three-dimensional reconstruction.

Keywords: Scanning Electron Microscopy, 3D Reconstruction, FEM Simulations, Photometric Method, Electron Trap

INTRODUCTION

Over the last few years functional surface structures have gained importance. For instance, the adhesion reducing so-called lotus effect or riblets-structures, which can decrease friction losses, have settled in many products. An essential property for a deliberate manipulation of these structures is the ability to perform precise three-dimensional non-destructing surface measurements. The following part presents the most commonly used methods. Fast measurement rates in the range of a few minutes per square millimeter can be achieved with the confocal microscopy or the white light interferometry, both of which are based on the visible light. Apart from the measuring rate, the most important feature of a microscopic device is the resolution. The lateral resolution, which was first described by Ernst Abbe, can be described by means of the following formula: $d = \frac{\lambda}{2n sin\alpha}$, where d is the minimal distance between two spots of the specimen which can still be separated in the depiction of the specimen; n is the refractive index between the medium and the front element of the lens system; λ is the wavelength of the used light and α is the half of the dihedral angle of the focused objective. Using visible light, this limit is around $200nm$. For a higher lateral resolution, it is necessary to use different microscopic methods like the Atomic Force Microscopy (AFM) or the Scanning Electronic Microscopy (SEM). Despite a better lateral resolution, which lies in the sub nanometer range, these techniques have severe disadvantages. The AFM uses a stylus tip which can be seen as a morphologic filter[1] and, therefore, does not always depict the surface correctly. Furthermore, the measurement speed is relatively low since a scanning procedure with a resolution of 512x512 lines takes around 20 minutes. In comparison, the SEM is a fairly quick measurement method with a large scanning area. Once the specimen chamber is evacuated, measurements in an areal range of square millimeters can be performed within a few minutes. However, there is a huge drawback when using the SEM: although the produced images have a strong topological contrast and give a spatial impression, they are only two-dimensional and contain no information about the heights of the observed structures. Nevertheless, there are some attempts to obtain three-dimensional measurement data from a SEM. In the last two decades of the past century, a research group, led by professor Reimer at the University of Münster, developed a basic photometric method to reconstruct surfaces. It is based on the fact that the emission yield of the secondary electrons depends on the

local inclination of the surface. Even though the method is based on a simple reconstruction algorithm, it is not widely spread since it has some major drawbacks. Another approach is the photogrammetric method, which uses images of the specimen at different tilting angles. Due to an effect called parallax movement,[9] surfaces with different heights appear to be moving horizontally from image to another. The higher a structure is or the more it is tilted, the further it moves during tilting. However, since a correlation between the images becomes harder with increasing tilt angle, the tilting is limited to approx. $\pm 5°$ to $\pm 15°$[2].[3] These small tilt angles result in low parallax movements and thus, the reconstruction becomes less accurate - especially for low variations of the height of the structures. The structure itself also has an effect on the result – if the surface is too even, no correlation between the different images can be found and a reconstruction cannot be realized. And since a correlation always has to be obtained from regions of the images, it is impossible to avoid low-pass filtering of the surface. The SEM itself needs no modification for this method; only a eucentric tilting of the specimen stage has to be feasible. In February 2012, Carl Zeiss Microscopy presented software for its electron microscopes which uses the four quadrant backscatter electron detector (BSE) for a three-dimensional reconstruction. Images can be reconstructed within a second and no modification of the SEM has to be done. However, this method has to be seen as a visualization tool and not as a measurement device since it is not accurate.

IMPROVED PHOTOMETRIC METHOD

Over the recent years, an improved photometric method was developed at the IMR. The method was primarily designed for a double detector system using two oppositely mounted Everhadt Thornley Detectors (ETD) and a rotatable specimen stage. Although it is based on the old photometric method of professor Reimer, it outperforms the major flaws of that technique. First of all, the old method was based on a surface-dependent parameter σ_0 which varies with the specimen composition. It is no longer a part of the reconstruction and, therefore, it is feasible without any prior knowledge of the specimen composition. Second, the old reconstruction is based on an emission yield, which behaves as a cos^{-1} of the local inclination angle of the measured specimen. However, this assumption is only true for high primary energies which have to be avoided for an exact reconstruction. This problem was solved for smaller energies by means of a signal normalization.[4] The third erroneous assumption is that the angular distribution of the secondary electron (SE) emission was believed to have a cosine form. A much better and now implemented distribution is a quantum-mechanic approximation.[8] The largest flaw of the old photometric method is definitely the assumption that all emitted secondary electrons can be detected by the secondary electron detectors (SED). This detection ratio is also called collection efficiency of the detector system and was assumed to be 100%. – However, it is a fact that the major part of the SE emission is absorbed by the electron gun, the specimen chamber or the specimen itself. This results in an efficiency which lies around 20-30% for normal single detector SEMs.[5] Furthermore, giving a rough estimation for the efficiency of such a double detector system, the efficiency was included in the reconstruction algorithm of the new photometric method.

A basic principle of the improved photometric method is the subdivision of the electron emission into three different zones (compare figure 1). The emitted electrons that can be detected by one of the ETDs describe zone 1. The electrons that hit the electron gun describe zone 3 and all other electrons which neither hit one of the detectors nor the electron gun describe zone 2. All the zones can be defined by two spanning angles, the azimuthal angle θ and the horizontal emission angle β of the electrons. These angles, some other device-specific constants such as the absorption coefficient of the electron gun, specimen-specific values and the signal intensity of the two detectors can be used to reconstruct the slope angle in the x and y direction of each point and, thus, the whole surface of the specimen. Therefore, these are not the signals of the detectors themselves which are relevant; it is rather the difference between the signals of the two oppositely mounted detectors. Using this difference, it is possible to reconstruct the slope angle in the direction of the detectors. Therefore, two measurements with a specimen rotation of 90° in between can be used for a complete surface reconstruction.

The following equations describe the signal relations k_x and k_y necessary for the determination of the specimen slope in the x- and y-direction. Where I_{1x} and I_{2x} are the signal intensites of the detectors aligned on the x axis; I_{1y} and I_{2y} are the signal intensities of the detectors aligned on the y axis; φ_x is the inclination angle of the specimen surface in the x direction; φ_y is the inclination angle of the specimen surface in the y direction; β is the half of the horizontal opening angle of zone 1; λ is the angle between the z axis and the normal to the tangent
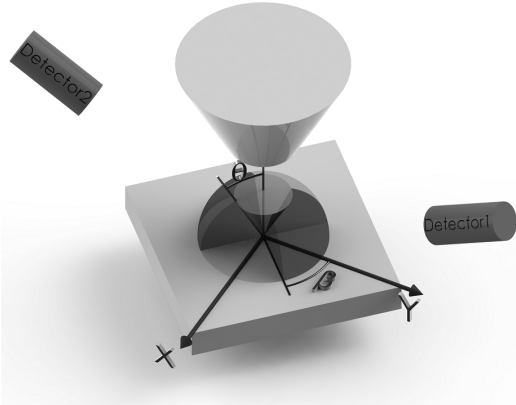
$$k_x\left(x,y\right) = \frac{I_{2x} - I_{1x}}{I_{2x} + I_{1x}}$$
$$= \sin\varphi_x \cdot \sin\beta$$
$$\cdot \frac{b_1 + b_2 \cdot \sin^2\varphi_x + b_3 \cdot \cos^2\lambda + b_4 \cdot \cos\lambda}{a_0 - a_1 \cdot \cos\lambda + a_2 \cdot \cos^2\lambda}$$

$$k_y\left(x,y\right) = \frac{I_{2y} - I_{1y}}{I_{2y} + I_{1y}}$$
$$= \sin\varphi_y \cdot \sin\beta$$
$$\cdot \frac{b_1 + b_2 \cdot \sin^2\varphi_y + b_3 \cdot \cos^2\lambda + b_4 \cdot \cos\lambda}{a_0 - a_1 \cdot \cos\lambda + a_2 \cdot \cos^2\lambda}$$

With:

$$b_1 = k_1 \cdot \left(1 + \tfrac{1}{\pi} \cdot \left(\sin\left(2\theta\right) - 2\theta\right)\right)$$
$$\quad - \tfrac{8}{3\pi} \cdot k_2 \cdot \left(1 - 3\kappa \cdot \cos^2\beta\right)$$
$$b_2 = k_2 \cdot \tfrac{8\kappa}{3\pi} \cdot \left(\sin^2\beta - 3 \cdot \cos^2\beta\right)$$
$$b_3 = -k_2 \cdot \tfrac{8\kappa}{\pi} \cdot \cos^2\beta$$
$$b_4 = k_2 \cdot \tfrac{8}{3\pi}\sin^3\theta$$
$$a_0 = 1 + k_2 \cdot \tfrac{1}{3\tau} \cdot \left(2 - 3 \cdot \cos\theta + \cos^3\theta\right)$$
$$a_1 = \tau \cdot k_1 \cdot \sin^2\theta$$
$$a_2 = \tau \cdot k_2 \cdot \left(\cos\theta - \cos^3\theta\right)$$

plane of the surface; $k1$ and $k2$ are the coefficients of the approximation of the quantum mechanics emission angle distribution; θ is the opening angle of zone 3 and τ is the absorption coefficient of the electron gun.

Figure 1: Zone splitting for a two detector system. Zone1: dark grey, zone2: light grey and zone3: transparent

As the equations above show, the complete reconstruction requires the signals of four detectors, which are equally spaced around the specimen. The unknown parameters like the opening angles θ and φ, which depend on the used SEM and its configuration, can be evaluated by means of the maximum likelihood estimation on measurement of a calibration sphere.
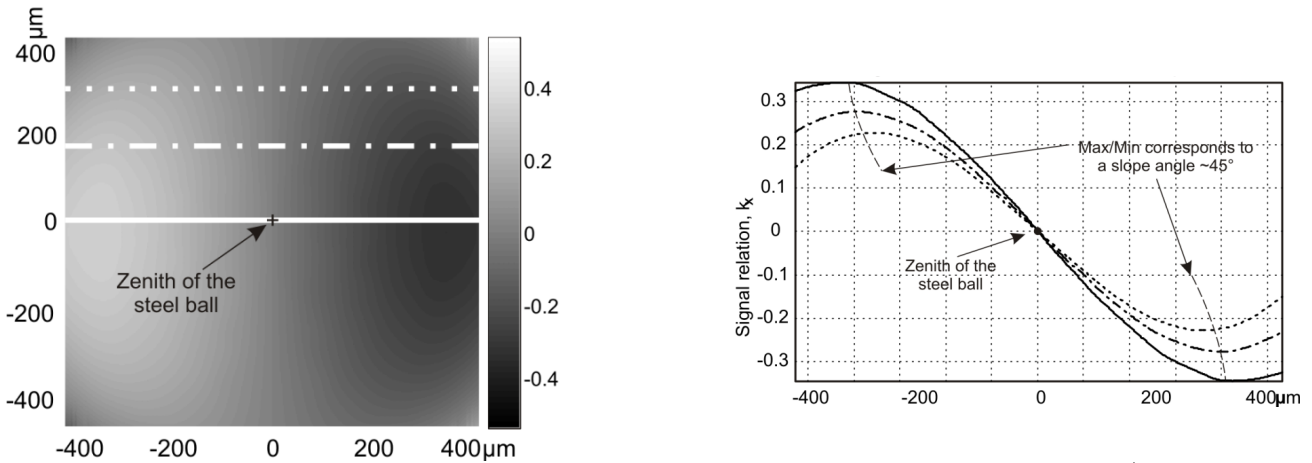
For a complete reconstruction, it is necessary to consider the influence of the surface, because concave structures can absorb electrons which are emitted in low angles. Therefore, the improved photometric method includes an iterative procedure using a Fast Fourier Transformation, which is capable of the reconstruction of such surfaces based on partially absorbed signals. A detailed explanation of that method can be found in in.[1]

The method was used on a modified Zeiss DSM 940A with two secondary electron detectors. Measurements on a calibration sphere with a diameter of 1mm showed the capability of a reliable reconstruction of that sphere up to a slope angle of approx. 45°. As figure 2 shows, the signal relation k_x becomes ambiguous on steeper surfaces, which makes a dependable reconstruction impossible.

DESIRED CHANGES AND FURTHER CONSIDERATIONS

In spite of the fact that this method corrects the major drawbacks of the classic photometric method, it is possible to perform some modifications to the employed SEM in order to further optimize the reconstruction. The method assumes that electrons, whose initial velocity lies within the detection zone of one detector, will definitely hit that detector. As simulations have shown, this is not always the case. The suction effect of the collector grids electric field is strongly connected to the geometry of the used grid. Since the grid of most standard SEMs is made of thin bendable wires, the geometry is not defined and, thus, the suction effect of two detectors is not equal, even if the collection voltage is the same. This led to the assumption that even if the initial velocity of an electron lies in a detection zone of a detector, it can't be guaranteed that it will hit that detector. This assumption was empirically proven in FEM-Simulations. Hence, a homogenous electric field distribution which does not affect the horizontal direction of first part of the electron trajectories is a desirable feature which should be used in the employed SEM. As shown in figure 2, the maximum detectable slope angle is
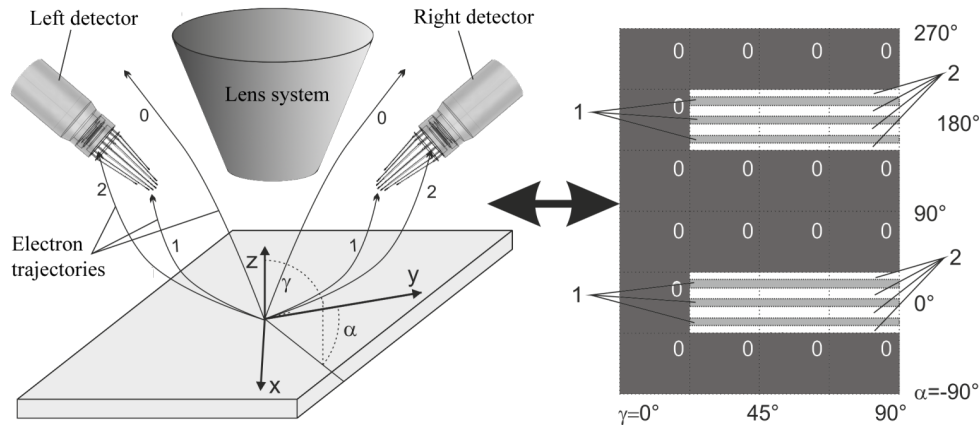
Figure 2: Signal relation k_x of the steel ball - overview (left) and chosen profiles (right)[4]

limited by the signal relations k_x and k_y, which are functions of the spanning angles for zone 1 (for zone splitting see chapter Improved Photometric Method). A further optimization is the increase of the collection efficiency and, thus, an enlargement of those spanning angles and the maximum detectable slope angle. It is also possible to drastically reduce the measurement time and complexity. Up to now, two measurements with a specimen rotation of 90° in between were necessary for a complete reconstruction. This is explained by the fact that the signals of two detectors are needed for a reconstruction of the partial derivation in one direction and the system only has two detectors. The rotation procedure is very time-consuming since it is not automated. Furthermore, both measurements have to depict the exact same region of the specimen, which is almost not feasible for large magnifications.

FEM SIMULATIONS

Basic principle

Figure 3: Schematic depiction of a two detector system with corresponding detection matrix[4]

Since the FEM simulations play an important role in the determination of the collection efficiency and, thus, the optimized design of the collector grid, it is necessary to explain the basic principle of these simulations. The basis of each simulation is an exact CAD model of the current modification of the SEM specimen chamber. The models were created with the CAD software Solidworks 2012 and were later imported to the FEM software COMSOL Multiphysics. The constraints such as the electric potentials of the grid and the scintillator discs were set. After applying a tetrahedral mesh to the model, a solution for the electric field distribution was computed. This solution was then used to determine the trajectories of electrons emitted from the center of the specimen.

The initial velocity of the electrons was set according to the energy of $7eV$, which corresponds to the centroid of the area below the secondary electron distribution, which can be calculated by $N(E) \propto \frac{E}{(E+\Phi)^4}$,[6] where E is the energy of the SE and Φ is the work function of the used material (Fe: 4.67[7]). In order to cover all possible emission directions, the emission vector was varied over a directional range of $360°$ (α) horizontal and $90°$ (γ) vertical, see figure 3. For the used timestep a constant value of $5 \cdot 10^{-12}s$ was chosen, since the beginning of each trajectory is important and has to be very exact and the electrons can reach high energies and thus velocities at the end of the trajectories. The used timestep leads to stepsizes of $7.8\mu m$ at 7eV (energy in specimen area) and $265\mu m$ at $8keV$ (energy in scintillator area). The trajectories were then exported to text files, which were later analyzed with Matlab to see which emission directions could be detected and which not. As already assumed in chapter "Improved Photometric Method", it was found that the emission directions could be grouped into three zones, which can be described by two spanning angles. In order to display those zones, detection matrices were introduced (see figure 3), in which each element stands for one emission direction. Depending on the end point of each electron trajectory, the color of the corresponding entry was either set to white (electron detected), grey (electron absorbed by grid) or black (electron not detected).
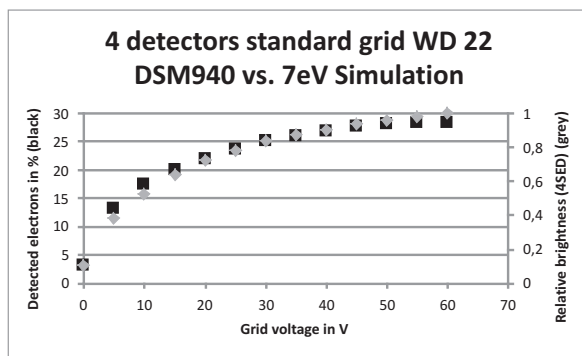
Verification of the simulation

Supplemental modifications of the SEM which will be described later are not the only measures to increase the collection efficiency. Also already build-in functions like the alternation of the working distance or the adjustment of the collector grid potential have an effect on the collection efficiency. To verify the simulations two tests were carried out comparing a model of a four detector system to a real four detector system regarding their collection efficiency. Since this test is – unlike to the prior described test – not used for determining the detectable emission directions rather used for a comparison between reality and simulation, the emission of the electrons has to be depicted according to the reality. Therefore the quantum mechanics distribution[8] was used for the angular distribution of the emitted electrons. It was implemented by adding a half sphere with a diameter of $8\mu m$ to the origin of the model. The electrons were emitted orthogonally to the sphere surface with a density according to the following formula
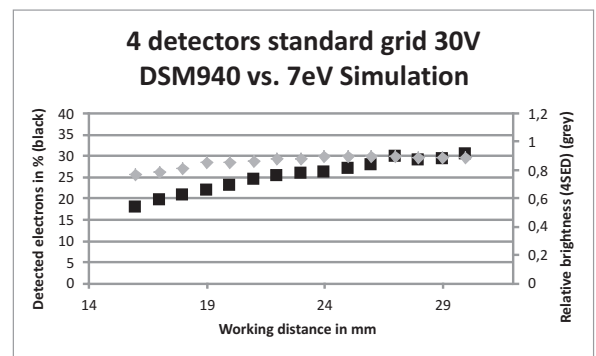
$$\frac{1}{Density} = \sqrt{r^2 - z^2} \cdot \left(\left(\frac{1}{\Pi} \right) \cdot \left(\frac{1.34 \cdot z}{r} - \frac{0.68 \cdot z^2}{r^2} \right) \right),$$

where r is the sphere radius and z the height of the emission origin of each electron.

In the first test the grid voltage for a four detector system with standard grids was varied over a range from $0V$ to $60V$. For the simulation the fraction of the emitted electrons that could be detected by the scintillator discs was calculated. For the real system the signal of all four detectors was summed and normalized to its maximal value. The results for a working distance of $22mm$ can be seen in figure 4. Both tests show quite a similar course.

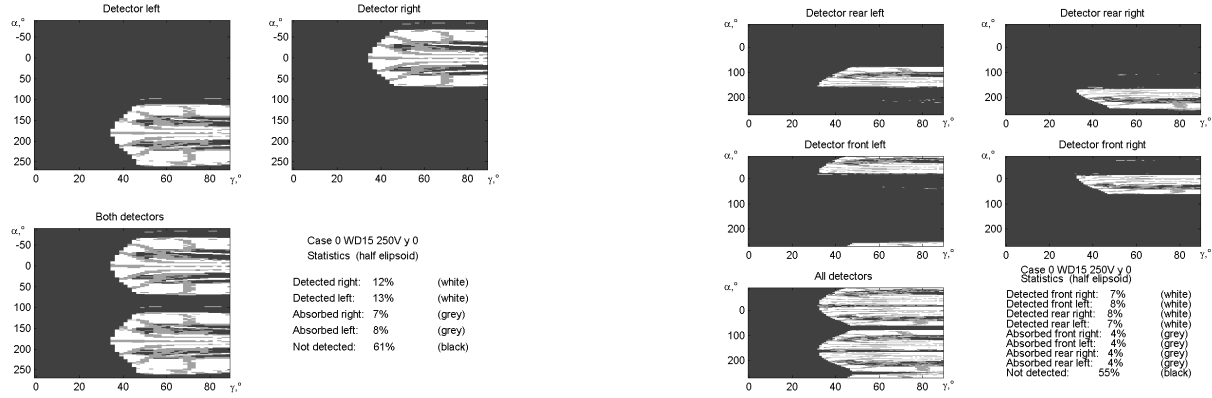**Figure 4:** Simulation results with four standard detectors and a working distance of $22mm$

Figure 5: Measurements results with four standard detectors and a working distance of $16mm$

In the second test the working distance was varied over a range from $16mm$ to $31mm$ (see figure 5) while the grid voltage was set to 30V. The course for real test and the simulation looks similar.
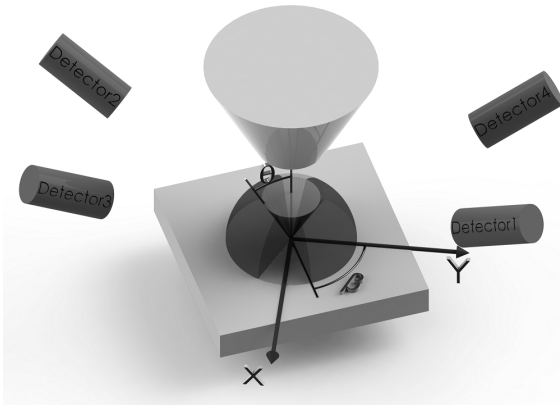
MODIFICATIONS TO THE SEM

Four detectors

To realize short measurement times, it is necessary to avoid the mentioned specimen rotation. Consequently, the used SEM was equipped with two additional identical detectors.

Figure 6: Detection matrix for a two detector system (left) and a four detector system (right) with 250V grid voltage

Figure 7: Zone splitting for a four detector system. Compared to figure 1 an enlargement of zone 1 occured.

FEM simulations showed that the collection efficiency can be increased by using the four detectors up to approx. 30% in comparison to approx. 25% for a two-detector system (see figure 6). This can be explained by an enlargement of zone 1 (compare figures 7 and 1).

Cylindric Grid

As stated before, a homogeneous electric field distribution should be assured close to the specimen. Therefore a cylindric grid which surrounds the specimen was designed, laser welded and implemented. The grid consists of four steel (1.4310) rings and 8 steel (1.4301) rods. The rods ensure a constant spacing between the linearly positioned rings. To hold the cylinder in a fixed position, each of the four SED is connected by means of 10 steel (1.4301) connection wires to the grid. Another feature of the connection wires is the 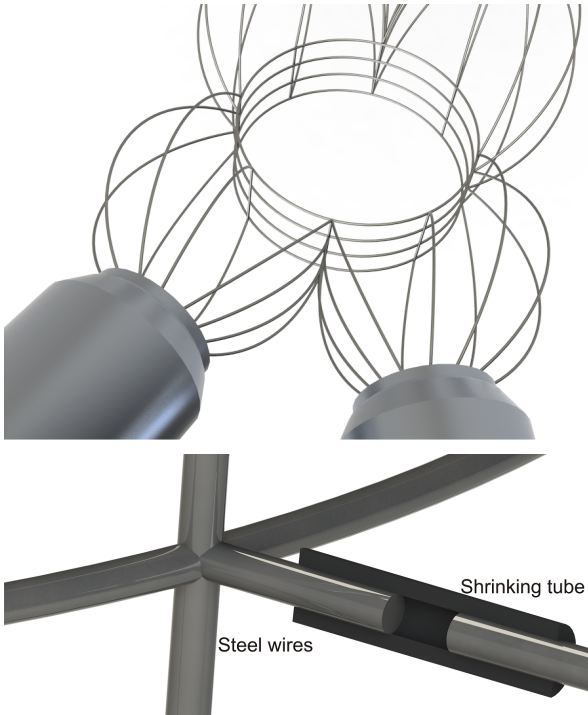channeling of all electrons towards the detectors. In the first approach of the designing process, the steel wires were planned unbowed. The simulation showed some unwanted effects and, subsequently, the connection wire design was changed to a bowed shape (see figure 8). To redirect the electrons, it is useful to be able to set the cylindric grid and the connection wires under different electric potentials. Hence, the connection wires needed to be isolated against the cylinder. Therefore, for each connection, approx. 3cm of shrinking tube were used to fix the endings of both wires. This way, it was possible to achieve mechanic stability while still having the wires electrically isolated (see figure 8). Figure 9 shows the grid just before its installation.
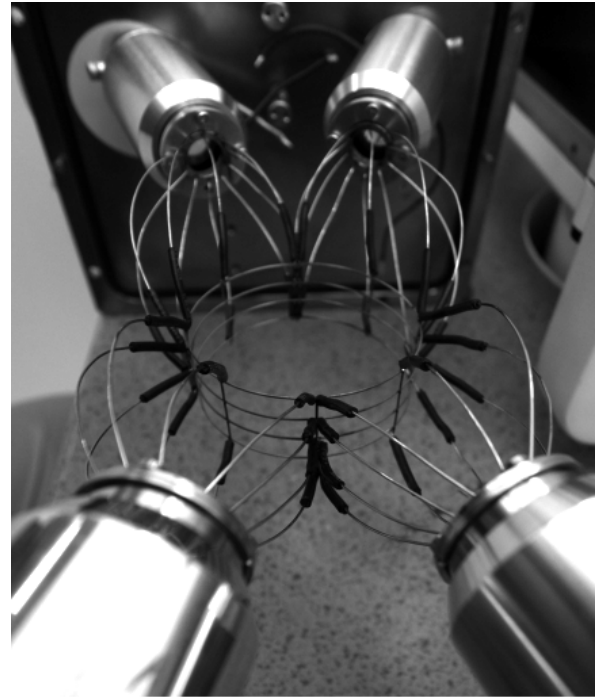
Measures to further enlarge the collection efficiency

The cylindric grid and the four detectors were mainly installed to ensure a homogenious electrical field distribution close to the specimen. A desired side effect was the increase of the collection efficiency. But there are several measures to enlarge the fraction of detectable electrons and thus the collection efficiency of the system. In the following passage a brief description will be given.

Figure 8: CAD drawings of newly designed grid. Whole grid with bowed connection wires (top) and cross section from shrinking tube connections (bottom)
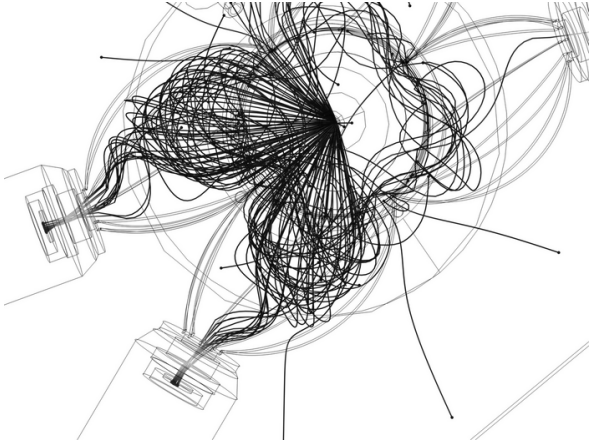

Figure 9: The newly developed cylindric grid just before the installation into the Zeiss DSM 940A.

Electron gun shielding As already mentioned, a large portion of all emitted electrons hits the bottom of the electron gun. In order to redirect these electrons towards the detectors, a shielding of the electron gun was introduced. The shielding device is a round disc with a diameter of 32mm and a central bore with a diameter of 7mm. It consists of a conducting copper layer and an isolating layer made of fiber reinforced plastic. The isolating layer is glued onto the electron gun so that the conducting copper layer faces the specimen. Using a soldered wire, a potential between 0V and -30V is applicable to the copper layer. By means of this technique, it is possible to redirect the major part of all the SEs. However, since the energy of backscattered electrons (BSE) can be close to the excitation energy of the primary electrons and, therefore, is significantly higher than the energy of the SE, it is impossible to redirect the BSE using this voltage range. Thus an electron trap will be introduced in a later chapter.
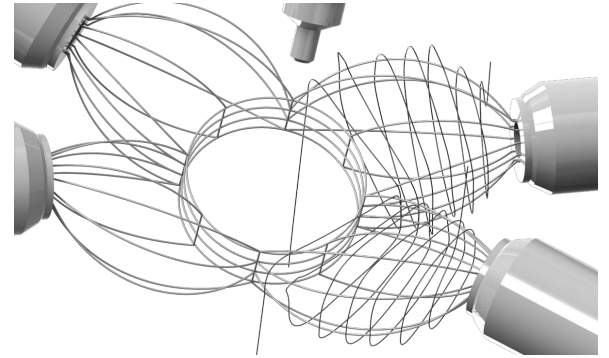
Optimization of the collector grid and the connection wires As the simulations show, the connection wires improve the collection efficiency. However, figure 10 also shows that the electrons which get close to the inner wires are led away from the detectors. Hence, the electric field is too strong in that region and has to be reduced. The reduction was achieved by reducing the number of wires in that region. It was determined that the optimal wire design consists of eight instead of ten connection wires per detector while the wires are bend with a smaller radius (see figure 10).

Adjustment of the cylinder and the connection wire voltages To determine the optimal voltages in the simulation a parametric study, in which the voltages of the cylindric grid, the connection wires and the gun shielding were modified. The cylindric grid voltage was modified over a range from 0V to 70V with an increment of 2V, the connection wire voltage was modified from -5V to 0V with an increment of 0.1V and the gun shielding had either -2V or -1V. The solutions for all possible parameter combinations with the trajectories of 120 electrons were computed and displayed. This way, it can easily be seen which combinations promise the best collection efficiency. These parameter combinations will be evaluated on the real SEM in later tests.

Figure 10: Top view on the simulation results for 120 electrons with cylinder: 38V, grid: -4V and gun shielding: -2V with 10 connection wires per detector on the left and 8 connection wires per detector on the right

Magnetic lenses Besides varying the potentials a magnetic lens was implemented in the simulations in order to redirect the electrons. The lens consisted of a thin wire, which was wrapped around two of the four connection wire sets (see figure 11). Seven currents between and including 0A to 1A were tested. Even in the direct comparison between the two models, which have the same constraints except the coil current –which is in one case 0 A and in the other 1 A – , there is almost no noticeable effect. This effect was also proven analytically for a coil with a diameter of 4.6cm, a length 4cm and 6 windings, which resembles the used coil. The calculations showed that the coil with a current of 1A only channels the electrons which have an angle of 20° or less between their initial direction and the centerline of the coil. Besides, having an additional magnetic field will always have effects one the primary beam and thus shall be avoided.
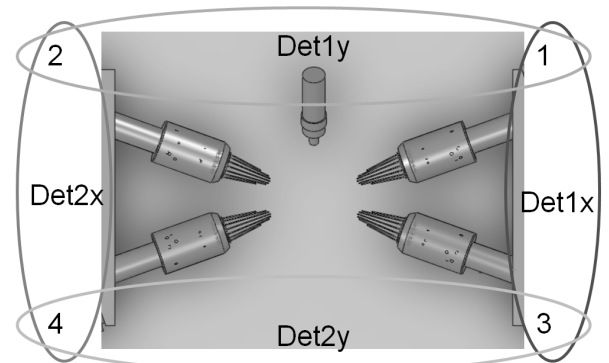

Figure 11: Four detectors with cylindical grid, bowed connection wires and two coils

SIGNAL MIXING

As stated above, the signal of two oppositely mounted detectors can be used to reconstruct the partial derivation of the surface in one direction. Therefore, for a complete reconstruction it is necessary to have the signals of

Mixing of the detector signals	Detection purpose
$Det_{1x} = Detector1 + Detector3$	Local inclination
$Det_{2x} = Detector2 + Detector4$	in x-direction
$Det_{1y} = Detector1 + Detector2$	Local inclination
$Det_{2y} = Detector3 + Detector4$	in y-direction

Table 1: Distribution of signal mixing

Figure 12: Schematic picture for signal mixing
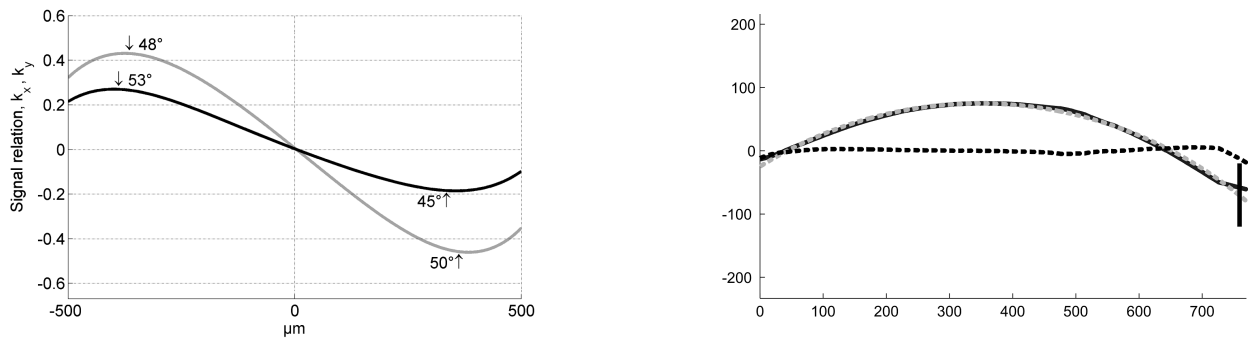
four detectors constantly spaced over a rotational angle of 360°. Due to the design of the specimen chamber, the angle between the two old and the two new detectors is limited to 42°, see figure 12. To still be able to use the reconstruction method on four detector systems, a signal mixing will be introduced. Therefore, the signals will be combined as shown in table 1. By means of the signal mixing it is possible to achieve higher collection efficiencies for the detection of the local inclination in one direction than using only two detectors. This also improves the accuracy and the robustness of the reconstruction method, with the mathematical model of the method still being valid for such a system.

MEASUREMENT RESULTS

In the following chapter some measurement results are shown for the four detector system with standard grids and the cylindric grid. Both tests were carried out with the newly developed signal mixing.

Four detectors - standard grid

The described enlargement of zone 1 could also be seen on the signal relations k_x and k_y for the four detector system with a standard grid. The ambiguity occures approximately at slope angles of ca. 50° which is 5° more than before (compare figures 2 and 13). Moreover, measurements of a calibration sphere proved that effect, because it is also possible to reconstruct slope angles up to 51° (see figure 13).

Figure 13: Results with 4 standard detectors on a $1mm$ calibration sphere. Left plot: k_x (black) and k_y (grey) with maximal detecable slope angle. Right plot: cutline of reconstruction result; recontruction (continuous line), real sphere (dashed grey), deviation (dashed black), deviation reaches limit of 1.8% at a slope angle of 51° (vertical line)

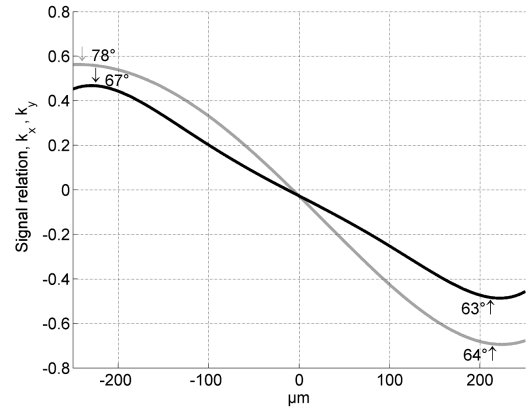### Four detectors - cylindric grid

ELECTRON TRAP

Even though the gun shielding shows the desired effect of redirecting some of the electrons, BSE can still pass the electric field and emit SE3 in the gun area. Thus an electron trap shall be invented which catches incoming BSE and thus reduces SE3 emission. First a simulation software to determine the optimal structure was developed and then some tests were run on manufactured structures.

Simulation software

In order to suppress the unwanted SE3 emission at the bottom of the electron gun an electron trap is introduced. The basic idea is that the electron trap catches the incoming BSE and only emits a small amount of SE3. It is assumed that the best structure consists of electrically conducting spikes with a high aspect ratio, which are distributed over the whole surface. Although the basic geometry of the nano-structure is committed, factors like the height (h), the spike thickness (b), thus the exact aspect ratio (h/b), the gap size (a), and the raw material or additional coatings have to be considered (compare figure 15 for dimensions).
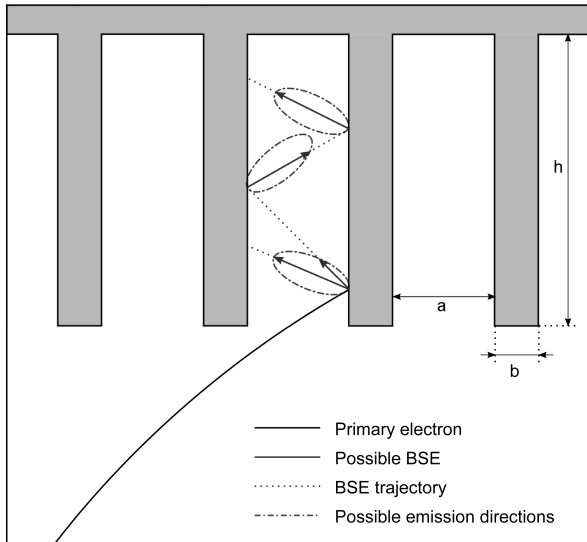
To determine all necessary details a simulation software was developed in C++. It is able to simulate SE and BSE emission of materials according to the energy and angle of incident electrons. The software computes the

Since the simulation results for the cylindric grid promised a high collection efficiency real measurements were perfomed using the optimized grid. The measurements of a calibration sphere with a diameter of $500\mu m$ show very good signal relations (see figure 14). Please note the maxima of the signal relations in comparison to figure 2 and figure 13. For the cylindric grid the maximal detectable slope angle lies in the range of $63°$ to $78°$. Since this is an increase of approximately $20°$ we assume that the recontruction of specimens will be a lot better using the cylindric grid. Please see upcoming publications for further results.
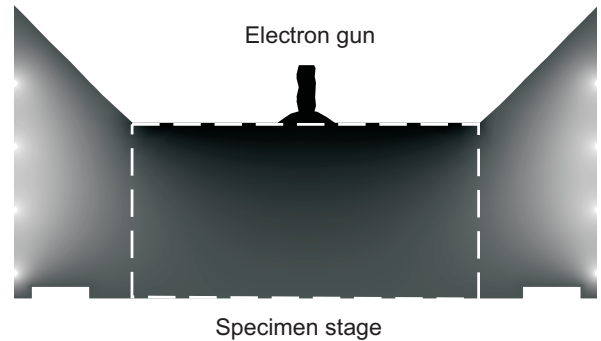

Figure 14: Signal relations for a $500\mu m$ Tungsten Carbide sphere measured with a four detector system with a cylindric grid. k_x marked in black and k_y in grey with maximal detecable slope angle.

emission yield, the energy distribution and the angular distribution of emitted SE and BSE according to the energy and direction of incident electrons. In that way all electrons can be observed until their energy either reaches a lower bound or leaves the region of interest (ROI). The theoretical models for the computation of those parameters are not described in this paper. Please see upcoming publications for details. To use the most realistic constraints a model of the used SEM is implemented. The electric field and the geometry is imported from the formerly described FEM simulations. Therefore a map of the electric potential for a four detector system with a cylindric grid is exported from comsol with a resolution of 8 bit (see figure 16). The cylindric grid is set to 20V while the gun voltage has potential of -7V.

Figure 15: Basic structure of the electron trap with possible BSE emission. Please note that the lengths of arrows (shape of the emission zone) represent the probability of that specific direction and not the energy. Also note that SE emission is also computed but not shown in this picture.

Figure 16: Computed electric field distribution with marked ROI. Black corresponds to -7V and white corresponds to 20V (except specimen stage and electron gun).

For each test an electron beam which starts in the electron gun and points directly ontho the specimen stage is simulated. The beam has a specified number of electrons with an energy of $E = 2keV$. In order to determine the

optimal structure the tests can be parameterized with a large range for the parameters h, b and a. The value r calculated as the ratio between the number of electrons leaving the ROI for a test with an unstructured cannon and the number of electrons leaving the ROI for the current setup describes the quality of the electron trap. It is desired to be as small as possible. So far two tests were carried out.
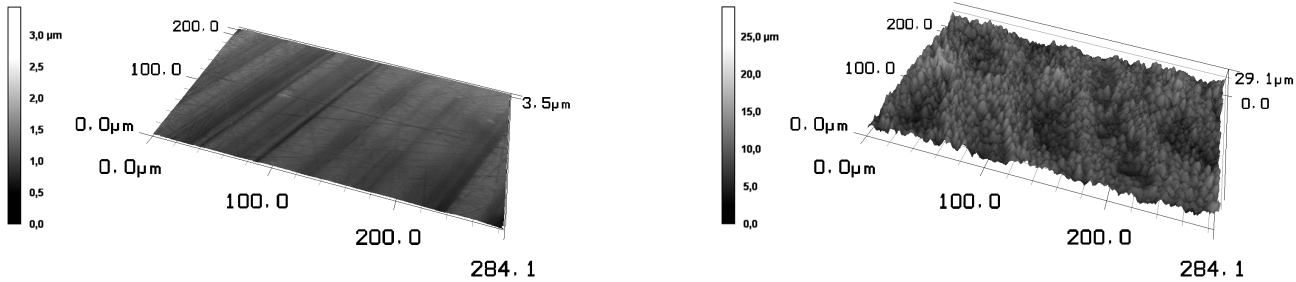
Setup	Height (h)	Electrons (m)	Ratio (r)
Even	0 μm	24500	1.000
Rect. 1	1 μm	29500	1.204
Rect. 2	2 μm	17000	0.694

Table 2: Simulation results for electron trap

In table 2 the parameters as well as the number of electrons leaving the ROI and the resulting ratio are listed. While the thickness was $b = 300nm$, the gap size was $a = 700nm$ and the number of emitted primary electrons was $n = 20000$ for all tests. It can be seen that r is larger than 1 for a structure height of $h = 1\mu m$ which is actually worse than the unstructured surface. But on the increase of the height by just one μm to $h = 2\mu m$ the ratio r already drops to $0.694\mu m$, which is a pretty good value.

Manufactured structures

Beside the simulation real structures were manufactured at the Fraunhofer Heinrich Hertz Institute in Goslar, Germany using a laser structuring process on a titanium sheet. In order to get a first impression of the capability this technique offers to produce an electron trap the structures were tested in a SEM and compared to an unstructured titanium sheet.

Figure 17: Unstructured (left) and structured (right) titanium surface measured with a confocal laser scanning microscope. Note that the waviness on left image due to manufacturing grooves is comparatively small.

During the tests the structures were scanned in regions of different sizes while the scanning parameters were held stable for both structures. The raw resulting signal was summed for each region. The tests were carried out for primary energies of $1keV$ and $2keV$ The following tables show the results.

Please note that only the ratios between the tests for 1keV and 2keV can be compared. The absolute brightness values can only be compared within each table since the gain settings were varied upon changing primary energy.
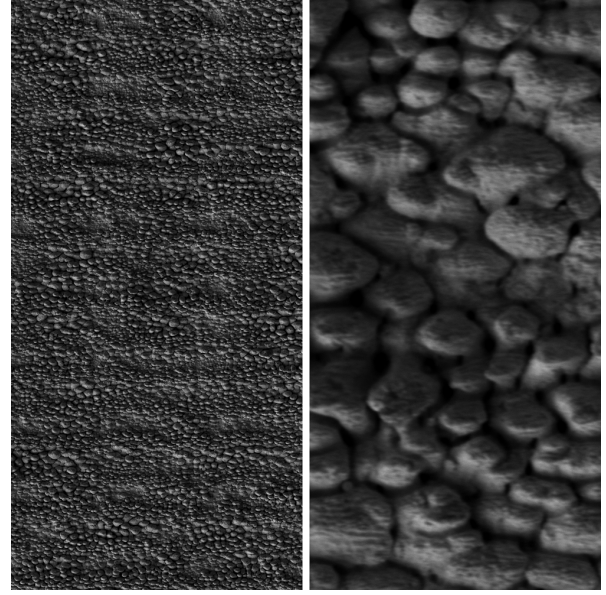
Again a ratio which is lower than one is desired. The tests show that this can be achieved using the structured titanium. It can be seen that the results are better for lower primary energies, which can be explained by the sub-nanostructures on the surface of the actual electron trap. It is assumed that electrons of higher energies are able to permeate those structures which leads to an increased emission area. The ratio is also very unstable for regions of different sizes. This can be explained by the geometry of the structures and their distribution. The distribution is not homogeneous, there are areas with a high absorbtion rate and some with a lower. If the observed area is too small the result (here the ratio) is not statistically representative (compare figure 18.

CONCLUSION

In this paper the main benefits of the new photometric method for a three dimensional reconstruction of SEM measurement data are described. Although this method outperforms the major drawbacks of the old photometric method its development is not complete. Due to modifications made to the employed SEM like the installation

1 keV			
Area in μm x μm	Intensity		ratio
	even	structured	
1887x1887	20592	16407	0.80
943x943	19179	16579	0.86
472x472	17417	16469	0.95
189x189	15021	15347	1.02
94x94	13902	14312	1.03
47x47	13295	12967	0.98
19x19	13429	12313	0.92
2 keV			
Area in μm x μm	Intensity		ratio
	even	structured	
1887x1887	19034	17270	0.91
943x943	17746	16954	0.96
472x472	15827	16700	1.06
189x189	14323	16046	1.12
94x94	13138	15145	1.15
47x47	12956	13919	1.07
19x19	13115	12320	0.94

Table 3: Measurement results

Figure 18: SEM images of the electron trap in two magnifications. Left: $943\mu mx470\mu m$ right: $94\mu mx47\mu m$. Dark zones represent a good ratio.

of two supplemental electron detectors and a custom collector grid the maximal detecable slope angle could be increased from 45° over 50° with 4 standard detectors to approx. 65° with a cylindric grid. The shape and potential of the new grid was created with the aid of detailed FEM simulations. The extensive model could also be verfied with tests on a real SEM. The results from the simulations were displayed using detection matrices. Besides these modifications an electron trap was introduced. It has the potential to further increase the quality of the reconstruction. For the optimal dimensioning of the trap a simulation software was written and some structures were tested. Also real structures with electron catching properties were produced and tested in a SEM.

OUTLOOK

In further work the current calibration sphere will be reconstructed from measurement data using the cylindric grid. Besides this measurement also other samples shall be reconstructed and compared to each other to see strengths and limits of this technique. Also a new specimen holder especially designed for the calibration of the four detector system using these algorithms will be introduced. As a further optimization a double layer specimen coating will be considered. It shall achieve a high SE output while the BSE output stays low. For the electron trap new manufacturing techniques will be employed and further testing of different structures will be performed.

ACKNOWLEDGEMENT

REFERENCES

[1] Vynnyk, T.: REM-Topografiemessungen an mikro- und nanostrukturierten Oberflächen, Dissertation, Shaker Verlag, Aachen 2010

[2] Alicona Imaging GmbH: `http://www.alicona.com/home/fileadmin/alicona/sidebar_left/Alicona_Mex.pdf`

[3] Hemmleb, M.: Photogrammetrische Auswertung elektronenmikroskopischer Bilddaten, Dissertation, Berlin, 2002

[4] Vynnyk, T.; Scheuer, R.; Reithmeier, E.: 3D-measurement using a Scanning Electron Microscope with 4 Everhart-Thornley Detectors, Proceedings of SPIE, 0277-796x, v. 8036, Bellingham, Washington, 2011

[5] Müllerova, I.; Konvalina, I., Collection of secondary electrons in scanning electron microscopes, Journal of Microscopy 233, 203-210, 2009

[6] Hopster,H.; Oepen, HP., Magnetic Microscopy of Nanostructures, Book, Springer Verlag Heidelberg, p. 141, 2005

[7] David R. Lide, ed., CRC Handbook of Chemistry and Physics, Internet Version 2005, P. 12-124, ¡http://www.hbcpnetbase.com¿, CRC Press, Boca Raton, FL, 2005

[8] Cazaux, J., Recent developments and new strategies in scanning electron microscopy, Journal of Microscopy 217, 16-35 (2005)

[9] Xie, J., Stereomicroscopy: 3D Imaging and the Third Dimension Measurement, Application Note, P. 4-7 (2011)